Toward an understanding of magnesium in a biological environment: A density functional theory study

RESEARCH ARTICLE | JUNE 01 2026

Toward an understanding of magnesium in a biological environment: A density functional theory study

Miranda Naurin ; Sally Aldhaim; Moltas Elliver; Ludwig Hagby ; J. Didrik Nilsson ; Elsebeth Schröder

AIP Advances 16, 065004 (2026)
https://doi.org/10.1063/5.0332131

Toward an understanding of magnesium in a biological environment: A density functional theory study

Cite as: AIP Advances 16, 065004 (2026); doi: 10.1063/5.0332131
Submitted: 7 April 2026 • Accepted: 11 May 2026 •
Published Online: 1 June 2026

Miranda Naurin, Sally Aldhaim, Moltas Elliver, Ludwig Hagby, J. Didrik Nilsson, and Elsebeth Schröder[a)]

AFFILIATIONS

Department of Microtechnology and Nanoscience, MC2, Chalmers University of Technology, SE-41296 Göteborg, Sweden

[a)]Author to whom correspondence should be addressed: schroder@chalmers.se

ABSTRACT

Density functional theory is used to investigate the interactions between a layer of magnesium hydroxide, $Mg(OH)_2$, the magnesium (Mg) surface Mg(0001), and the three amino acids glycine, proline, and glutamine. The aim is to improve the understanding of Mg behavior in biologically relevant environments, such as the ones that biodegradable implants experience in the body. For a simple model of such conditions, the adsorption of amino acids is studied. With the layer of $Mg(OH)_2$ as a model of either slightly corroded Mg or intentionally coated Mg, the interfacial interaction between a layer of $Mg(OH)_2$ and Mg(0001) is first examined in the absence of the molecules. Then follows analyses that include amino acids on top of the $Mg(OH)_2$ layer. We find that the $Mg(OH)_2$/Mg(0001) interaction is weak and that the layer of $Mg(OH)_2$ can readily slide across the Mg surface. The presence of amino acids is found to have a limited influence on the adsorption of $Mg(OH)_2$ on Mg(0001), decreasing the binding by at most 3%, while more layers of $Mg(OH)_2$ strengthen the $Mg(OH)_2$/Mg(0001) binding by 13%. This is still less than the binding of $Mg(OH)_2$ layers within its native bulk structure, and our findings indicate that only a small number of hydroxide layers are required before it is energetically more favorable for $Mg(OH)_2$ to create bulk than to stay on Mg(0001) as single layers. This provides insight into early-stage surface processes relevant for magnesium-based implant materials.

I. INTRODUCTION

Popular implant materials, such as steel and titanium alloys, can provide stable fixation with high mechanical strength.[1] However, for bone healing, high strength in the implant is not necessarily an advantage; for example, titanium alloys can cause stress shielding to the bone, removing most of the stress that the bone would otherwise be subjected to. This could cause the bone to evolve more slowly as it needs to be exposed to some stress to strengthen. Moreover, if the implant is intended as a temporary support, the implant must be removed in an additional surgery because these materials are not biodegradable.[2] This comes with several risks for the patient and an additional cost for society.

Magnesium (Mg) is a candidate for a biodegradable implant material. It is the fourth most abundant metal in the human body, most of which can be found in the skeletal system.[3] Previous studies have demonstrated that Mg implants have good biocompatibility and do not harm bone generation,[4] and *in vivo* testing has shown that Mg ions may induce bone formation.[5] Mg has a density similar to that of bone,[2] while the density of titanium alloys is significantly larger.[6] Furthermore, the mechanical properties of Mg are close to those of bone; for example, *in vitro* studies have shown the elastic modulus of Mg and bone to be similar.[7]

The use of Mg as a biodegradable implant was first introduced in 1906,[5] but use was abandoned due to the high corrosion rate that resulted in excessive production of bubbles of hydrogen gas (H_2). On the one hand, the released H_2 gas *in vivo* is believed to affect the integration of the implant with the surrounding bone tissue,[4] and the gas bubbles can occupy space and potentially induce local mechanical pressure. These bubbles can lead to shifts in the acidity of the surrounding environment, with the risk of negatively affecting the early stages of bone healing, particularly in the outer

bone tissue. On the other hand, a recent *in vivo* study conducted on rats[8] indicated that such effects might not be critically detrimental. Despite elevated degradation rates and substantial hydrogen evolution, complete bone regeneration was still achieved.

Still, the stability and mechanical properties of the implant must be preserved for a certain period of time on the scale of a year. With this in mind, controlling the corrosion rate of magnesium is of high priority and a necessary step toward making magnesium-based biodegradable implants. Approaches to inhibit the corrosion include the alloying of Mg or coating the Mg surface with a less reactive material.[3,7,9] The goal is to inhibit the degradation of the implant just enough for stability during bone growth and still sufficiently rapid degradation afterward.

In this work, we use density functional theory (DFT) calculations to study the adsorption of a layer of magnesium hydroxide, $Mg(OH)_2$, on top of the Mg(0001) surface, modeled as an intentional coating or as a result of the first stages of Mg oxidation. We determine the energy needed to peel off the $Mg(OH)_2$ layer directly and the energy needed to slide the layer across the Mg surface, which would eventually lead to the layer sliding off the Mg surface. Furthermore, we calculate the adsorption energies and geometries of the body-relevant amino acids glycine (Gly), proline (Pro), and glutamine (Gln) on this coating, and study how they influence the binding of $Mg(OH)_2$ to Mg(0001).

The text is organized as follows: Section II introduces the methods used and materials studied, Sec. III contains our results, including discussions, and conclusions and a summary are given in Sec. IV. Finally, in the Appendix, we discuss the convergence of central parameters in the calculations.

II. METHODS AND MATERIALS

A. Density functional theory calculations

DFT is used to calculate the structures and energies of the adsorbed coating and amino acid molecules. We employ the plane-wave code `pw.x` of the Quantum ESPRESSO suite,[10–12] with exchange and correlation approximation given by the vdW-DF-cx method.[13–16] Since some of the adsorption is expected to be weak, it is important to use an approximation that self-consistently includes dispersion, or van der Waals (vdW) interactions, such as vdW-DF-cx. The vdW-DF-cx has current conservation as guidance and has been shown to work excellently in the adsorption of organic molecules.[16,17]

We use PAW-based[18] pseudopotentials (PP) that were all created by the `ld1.x` code[19] of Quantum ESPRESSO. For Mg, we use the two-valence-electron PP Mg-pbesol-paw-3d.UPF, created and tested in Ref. 20, while all other PPs are from the PSLibrary package.[21]

As described in the Appendix, we tested and found that a dense (more sparse) Monkhorst–Pack[22] k-point mesh with $18 \times 18 \times 1$ ($10 \times 10 \times 1$) points in the 1×1 surface cell is sufficient for an accuracy in energy difference of 0.03 meV/Å^2 (0.3 meV/Å^2). For all calculations of $Mg(OH)_2$ on top of Mg(0001), we use the dense mesh. For calculations of amino acid adsorption, we use the larger 5×5 surface cell. The structures and, thus, the adsorption energies of the molecules are inherently less accurate (due to multiple local minima in the energy landscape, of which we can never catch all). Therefore, it suffices to use the more sparse mesh for these calculations, corresponding to $2 \times 2 \times 1$ k-points in the 5×5 surface cell.

Similar tests for the cutoff energy values of the plane-wave kinetic energy E_{cut} and electron densities E^{ρ}_{cut} yield $E_{\text{cut}} = 50$ Ry and $E^{\rho}_{\text{cut}} = 400$ Ry for sufficient accuracy in the present project. For our graphene and graphite calculations, we use corresponding parameters. For more details on our convergence tests, we refer to the Appendix.

Unless otherwise stated, the atomic positions in the system are optimized such that the Hellmann–Feynman forces, obtained from the DFT-generated electron charge density, are minimized. This does not apply to the lower three Mg layers in the Mg(0001) surface, as explained in Section II B.

Finally, for testing a number of realistic starting configurations of the amino acid positions on the surface, we employed the molecular editor Avogadro[23] using (classical) molecular mechanics to obtain a series of fast, guided, initial guesses for the adsorption geometries, to use as input to DFT calculations with minimization of the Hellmann–Feynman forces to further optimize the atomic positions.

B. Surface and overlayer

$Mg(OH)_2$ is a known corrosion product of Mg surfaces in contact with a biological environment.[24–26] Therefore, it is expected to naturally be present on or near Mg-based implants, but it can also be part of an intentionally created coating.[27,28] At ambient temperature and pressure, Mg bulk condenses in a hexagonal closed-packed (HCP) structure. $Mg(OH)_2$ is a layered material that also has the HCP structure, with a lateral lattice constant only slightly smaller than that of bulk Mg. This means that we can place a layer of $Mg(OH)_2$ on top of Mg(0001) with the same periodicity, imposing only a minor strain on $Mg(OH)_2$.

When only $Mg(OH)_2$ is adsorbed on Mg(0001), we thus use a 1×1 surface unit cell of Mg(0001) (Fig. 1). However, when amino acid molecules are adsorbed on top, we use the laterally larger 5×5 surface cell to avoid spurious interactions of the molecules across the periodic boundaries. For the largest molecule studied here (Gln), the smallest distance between atoms on two periodic copies of the molecule is then 9 Å. The lattice constants of Mg bulk, with the PP used here, were found in Ref. 20, and thus, our 1×1 Mg(0001)-surface is created with lateral lattice constant $a = 3.192$ Å.

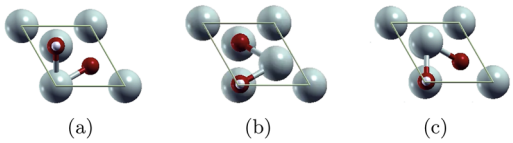

FIG. 1. $Mg(OH)_2$ on top of Mg(0001) in a 1×1 surface unit cell. (a) $Mg(OH)_2$ with the lower H atom above an FCC hollow site on Mg(0001) and Mg of $Mg(OH)_2$ above an HCP top site. (b) The optimal position for $Mg(OH)_2$, with H above an HCP hollow site and Mg above an FCC hollow site. (c) The lower H atom above an FCC hollow site and Mg of $Mg(OH)_2$ above an HCP hollow site. This position cannot be obtained by simply translating $Mg(OH)_2$ in (a) without rotations; the adsorption energy was separately calculated.

TABLE I. Our calculated energy differences for $Mg(OH)_2$ on magnesium and for graphene on graphite. $E_{ads}(\mathbf{r}_{opt})$ is the energy required to lift off the top layer from its optimal position, $\Delta E^*_{ads}(\mathbf{r}_{max})$ is the maximum difference in energy at the surface and, thus, the maximum energy that can be required for the top layer to slide, while column ΔE^*_{SP} shows the two lowest saddle points, indicating the minimum energy required for sliding. Values in meV/Å^2.

System	$E_{ads}(\mathbf{r}_{opt})$	$\Delta E^*_{ads}(\mathbf{r}_{max})$	ΔE^*_{SP}
Graphene on graphite	−25.3	3.7	0.4, 1.9
$Mg(OH)_2$ on magnesium	−17.9	5.7	1.1, 2.1

We model Mg(0001) using five Mg layers, of which the lowest three are kept in the positions they had in a fully relaxed 23-layer Mg slab.[20,29] All other atoms, including atoms of the overlayer and molecules, are allowed to relax, unless specified. For the direction perpendicular to the surface, we use a unit cell height of 36 Å, leaving at least 14 Å of vacuum even when amino acids are adsorbed. In the vacuum region, we impose a dipole correction to account for the top and bottom of the surface slab being different.[30]

For bulk $Mg(OH)_2$, we find the lateral lattice constant to be 3.130 Å (experimental value a = 3.15 Å[31]), which means that we must expand $Mg(OH)_2$ by 2% to fit a layer of $Mg(OH)_2$ on top of Mg(0001).

In our calculations of graphene on graphite for Table I, we use three layers of graphite as the surface, with atoms initially in the bulk structure and lateral lattice constant (layer separation) calculated to be a_{gr} = 2.465 Å ($c_{gr}/2$ = 6.567/2 Å). In various positions, one layer of graphene is added on top.

C. Adsorption energies

The strength of the binding of $Mg(OH)_2$ to Mg(0001), of the amino acids on $Mg(OH)_2$ on top of Mg(0001), and of graphene on graphite is quantified by the adsorption energy E_{ads}, which is defined as

$$E_{ads} = E_{full} - E_{surface} - E_{adsorbant}. \quad (1)$$

Here, E_{full} is the calculated total energy for the full system, and $E_{surface}$ and $E_{adsorbant}$ are those of the surface and the adsorbant. Depending on the adsorption energy of interest, the surface is either Mg(0001), Mg(0001) with $Mg(OH)_2$, or graphite(0001), and the adsorbant is either a $Mg(OH)_2$ layer (with or without an amino acid), an amino acid molecule, or single-layer graphene. For both $E_{surface}$ and $E_{adsorbant}$, we use the relaxed structures, allowing also $Mg(OH)_2$ to release the lateral strain that is imposed at adsorption, to fit the Mg(0001) lattice constant. With the definition in (1), binding is obtained for negative values of E_{ads}.

E_{ads} is the energy required to lift the molecule, the $Mg(OH)_2$ layer, or graphene directly from the surface. However, if the $Mg(OH)_2$ or graphene layer can slide on the surface, it might eventually slide off, possibly at a lower energy cost than directly lifting it off. Therefore, we also calculate the difference in E_{ads} for $Mg(OH)_2$ as the layer is moved across Mg(0001), creating a potential energy surface (PES) plot, as shown in Fig. 2. The largest difference in E_{ads} for any two positions of $Mg(OH)_2$ on Mg(0001), ΔE_{ads}, is an upper limit on the energy needed for sliding the layer, and together with

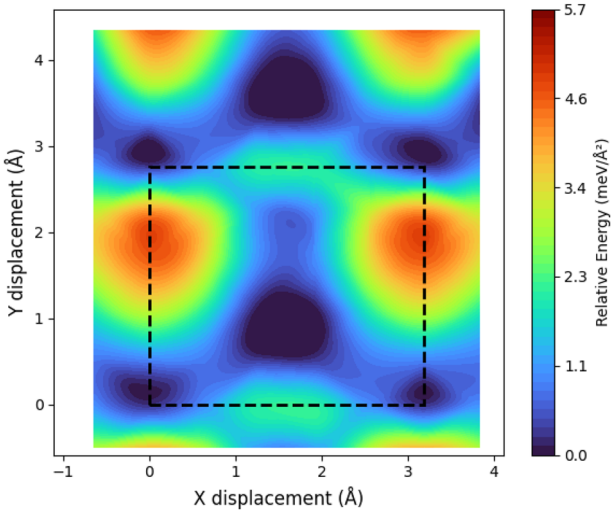

FIG. 2. Potential energy surface plot for a layer of $Mg(OH)_2$ translated across Mg(0001). The dashed black box illustrates the periodicity of the displacement. The energy is given relative to the optimal position. The optimal position, found in the dark-blue region close to the center of the dashed box, is the position shown in Fig. 1(b).

estimates of saddle point barriers, it can be taken as an estimate of the corrugation of Mg(0001) for $Mg(OH)_2$.[32]

For the PES plot, we need E_{ads} calculated for $Mg(OH)_2$ when translated across the surface, as well as when it is not in a (local) optimal position. Therefore, we keep the lateral positions of the atoms in $Mg(OH)_2$ fixed, to avoid the layer from sliding back to the (local) minimum during the optimization of the atomic positions. The layer is moved in equal increments in each lateral direction, resulting in 25 calculations within one unit cell of the Mg surface. In each lateral point on the surface, $\mathbf{r}_{\parallel}$, the two top layers of Mg atoms in Mg(0001) are free to move, while in $Mg(OH)_2$, the atoms are only free to move in the direction perpendicular to the surface. The adsorption energies thus found are estimates of the correct adsorption energies because the atoms of $Mg(OH)_2$ in the PES are restricted in their degrees of freedom. The PES is plotted with the energy scale relative to the adsorption energy in the optimal position $E_{ads}(\mathbf{r}_{opt})$ as

$$\Delta E^*_{ads}(\mathbf{r}_{\parallel}) = E^*_{ads}(\mathbf{r}_{\parallel}) - E_{ads}(\mathbf{r}_{opt}). \quad (2)$$

Here, $\mathbf{r}_{opt}$ is the fully relaxed optimal position of $Mg(OH)_2$ on Mg(0001), and the star indicates energies obtained when lateral positions of atoms in $Mg(OH)_2$ are not relaxed.

The same method is used for the values of graphene on graphite in Table I, with the optimal position in AB stacking.

D. Amino acids

We study the adsorption of three different amino acids on the $Mg(OH)_2$-covered surface. The molecules Gly and Pro are two common components of type-1 collagen. Type 1-collagen is one of the most common biomolecules in the human body, and it plays a crucial role in the formation of bodily tissue due to its highly stable triple-helix structure.[33] Each string consists of a repeating sequence

of the amino acids Gly-X-Y, where X and Y are various amino acids, most commonly Pro and hydroxyproline.

Collagen constitutes the primary component of the extracellular matrix, which is essential for bone tissue regeneration.[34] The extracellular matrix is the substance located between cells, which contributes to numerous biological functions within the body. Of particular relevance to this project, studies have demonstrated that Mg ions can bind to collagen, thereby promoting osteoblast differentiation through specific biological signaling pathways.[34] Osteoblasts are bone-forming cells responsible for stimulating the production of new bone tissue and are, therefore, critical in the regeneration process following a fracture.[35] Collagen also contributes to the structural integrity of both cartilage and bone, making its binding interactions with potential implants a subject of significant interest.

Gln is the third amino acid used in this project. In skeletal muscle cells, more than 50% of unbound amino acids are Gln,[36] and the skeletal muscle is the main tissue for Gln release, synthesis, and storage.[37] Hence, Gln is of high relevance to this project.

III. RESULTS AND DISCUSSION

We first focus on the adsorption of a layer of $Mg(OH)_2$ on Mg(0001) and the search for the optimal adsorption geometry. Thereafter, amino acid adsorption is discussed, along with the effect of this on the $Mg(OH)_2$/Mg(0001) binding, and finally, we discuss how alloying of the Mg surface might affect our results, based on previous work on Mg(0001) sparse alloying.

A. $Mg(OH)_2$ on Mg(0001)

For a layer of $Mg(OH)_2$ adsorbed on Mg(0001), one lateral unit cell of $Mg(OH)_2$ fits on one lateral unit cell of Mg(0001) if stretched by 2% in the lateral directions. However, we do not *a priori* know the optimal relative position of the $Mg(OH)_2$ layer because local atoms of the layer and the surface will interact.

The $Mg(OH)_2$ layer has a H atom pointing toward the surface. Previous studies have shown that, for a single atom of H adsorbed on Mg(0001), the energetically optimal position is in the FCC hollow site,[38,39] as also tested and found in the present study. Therefore, one might expect that the lateral position of the overlayer is such that the lower H of $Mg(OH)_2$ is above the FCC hollow site in Mg(0001), with two examples illustrated in Figs. 1(a) and 1(c). However, H as part of $Mg(OH)_2$ carries a different charge than a single H atom, with the major part of the electron density moving from H to the O atom in the O–H binding. Therefore, other relative positions may be more favorable.

We carry out a study to determine the adsorption energy E_{ads} in a grid of relative positions across the surface, as described below. The $Mg(OH)_2$ is translated in the lateral directions (without any rotation). By this, we obtain (an estimate of) the PES of $Mg(OH)_2$ on Mg(0001), as shown in Fig. 2. From the PES, we find that instead of H taking up the FCC hollow site, Fig. 1(a), the Mg atom of $Mg(OH)_2$ does. The optimal geometry is shown in Fig. 1(b), with the lowest H atom positioned above a second-layer Mg atom in Mg(0001), in an HCP hollow site. This position, $\mathbf{r}_{opt}$, corresponds to the darkest blue region in the PES plot.

Figure 2 shows that the adsorption energy differences are relatively small. We find that the largest energy difference is $\Delta E^*_{ads}(\mathbf{r}_{max}) = 5.7$ meV/Å^2, and the size of the two smallest saddle-point barriers ΔE^*_{SP} are 1–2 meV/Å^2, as shown in Table I. Comparing these values to the values for graphene on graphite shows that the layer of $Mg(OH)_2$ easily can slide off of the Mg surface, almost as easily as graphene on graphite. It also suggests stability against rupture due to strain for large patches on Mg(0001). It is a small cost to have parts of the patch sitting on less favorable positions, as will happen if the strain is partly released.

Based on the estimates of adsorption energies in Fig. 2, we calculate more accurate adsorption energies in the global minimum, corresponding to Fig. 1(b), and in the two structures corresponding to Figs. 1(a) and 1(c), now with the atoms of $Mg(OH)_2$ allowed to relax in all directions. We find the optimal adsorption energy, as defined by Eq. (1), to be $E_{ads} = -17.9$ meV/Å^2. This is a relatively small value compared, for example, with the energy cost of lifting off a layer of graphene from graphite, which we calculated to be −25.3 meV/Å^2, as shown in Table I. For the two other (metastable) structures, we find $E_{ads} = -17.1$ meV/Å^2 [Fig. 1(a)] and −17.6 meV/Å^2 [Fig. 1(c)].

Above, we studied the adsorption energy relative to a free-floating layer of $Mg(OH)_2$, with atomic positions and lateral lattice constant optimized. If we evaluate the energy relative to a layer of $Mg(OH)_2$ inside its bulk, we find the adsorption energy between the Mg-surface and $Mg(OH)_2$-layer to be +314 meV per surface unit cell, or +36.5 meV/Å^2, as further discussed below. The fact that the result is positive indicates that a layer of $Mg(OH)_2$ on Mg(0001) is not created spontaneously from the bulk. However, corrosion reactions can create $Mg(OH)_2$ and is a more realistic route to $Mg(OH)_2$ on Mg(0001). Furthermore, we see that, if, in the corrosion process, several layers of $Mg(OH)_2$ are formed, they bind more strongly to each other than one or more $Mg(OH)_2$ layers on Mg(0001). This is discussed further in Sec. III C.

Figure 3 illustrates energies involved in an imagined step-by-step process for creating a layer of $Mg(OH)_2$ from bulk. First, the layers would need to be separated, which is calculated as sketched in Fig. 3, going from (a) to (b). Subsequently, to fit with the periodicity of Mg(0001), the lateral lattice constant a of $Mg(OH)_2$ must be increased, as shown in Figs. 3(b) and 3(c). Finally, the layer is placed on Mg(0001), with relaxations of the atomic positions, as shown in Figs. 3(c) and (d). Each step except the last requires energy, as illustrated by the energies per lateral unit cell provided in Fig. 3. Our definition of E_{ads} corresponds to going from (b) to (d) in Fig. 3, while creating an overlayer from bulk $Mg(OH)_2$ requires the full cycle from (a) to (d).

As shown by the energies in Fig. 3, separating the layers of $Mg(OH)_2$ bulk costs the most energy. Some energy is gained when $Mg(OH)_2$ layers are placed on the Mg surface, but not sufficient for the whole process to be energy-efficient.

We also observe that changing the lateral lattice constant for $Mg(OH)_2$ from the bulk and free-floating value $a = 3.130$ Å to 3.192 Å of Mg(0001) barely has an impact on the energy, as shown in Figs. 3(b) and 3(c). This means that stretching the $Mg(OH)_2$ layer from its preferred lateral size does not have a significant impact on the system, thus confirming that it is reasonable to simplify the calculations by letting one unit cell of $Mg(OH)_2$ correspond to one surface unit cell of Mg(0001).

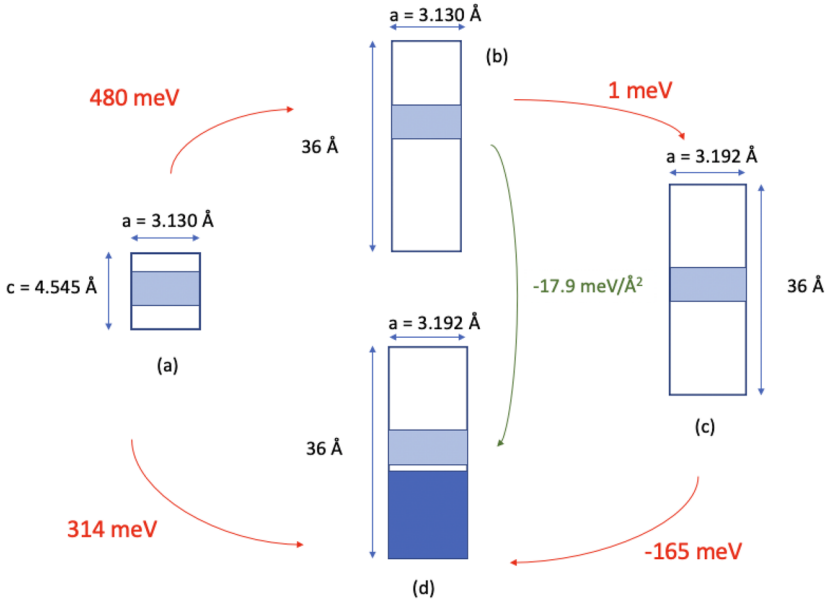

FIG. 3. Illustration of the energies that go into creating a $Mg(OH)_2$ layer on Mg(0001) either from bulk $Mg(OH)_2$ [(a)–(d)], or from an isolated layer of $Mg(OH)_2$ [(b)–(d)], in an imagined separation of the process. Light blue illustrates the $Mg(OH)_2$ layer, and dark blue illustrates the Mg surface. Values at the red and green arrows indicate the energy required to go from one step to the other. All energies in meV per surface unit cell, except the (b)–(d) energy.

B. Amino acid adsorption

We study the adsorption of single amino acid molecules on top of the $Mg(OH)_2$ layer, at low coverage [one molecule per 5×5 Mg(0001) unit cell]. In adsorption, both the molecule and the layer will adjust their atomic positions. We study this change in the geometry, in the corresponding energy changes, and in Sec. III C, we discuss the possible secondary effect of amino acid adsorption affecting the binding of $Mg(OH)_2$ on Mg(0001).

Table II shows, by the size of the deformation energies $E_{\mathrm{def}}^{\mathrm{amino}}$ and $E_{\mathrm{def}}^{\mathrm{surf}}$, that there is deformation both on the amino acids and on the surface when in contact, although mostly (as expected) when the molecule is strongly chemisorbed to $Mg(OH)_2$.

The largest impact on both the surface and molecule arises from the surface interaction with strongly chemisorbed Gly and Pro. At a closer look at the structures [Figs. 4(b) and 4(d)], we find that, in the two molecules, a H from the carboxyl group dissociates in the adsorption. On the other hand, the weaker adsorption of Gly and Pro [Figs. 4(a) and 4(c)], and the adsorption of Gln [Fig. 4(e)], does not give rise to any large deformations, although the deformation energy of the surface is larger than that of the molecule, especially for Pro. We judge this from the deformation energies in Table II and the adsorption structures in Fig. 4.

In the following, we discuss each of the amino acids and their adsorption properties.

TABLE II. Adsorption energy E_{ads} between the amino acid and the surface ($Mg(OH)_2$ on Mg), as well as the resulting deformation energy $E_{\mathrm{def}}^{\mathrm{amino}}$ and $E_{\mathrm{def}}^{\mathrm{surf}}$ of each component. "(weak)" and "(strong)" denote the weakly and strongly chemisorbed molecules. Values in eV per molecule.

Calculations	E_{ads}	$E_{\mathrm{def}}^{\mathrm{amino}}$	$E_{\mathrm{def}}^{\mathrm{surf}}$
Proline(weak)	−0.44	0.01	0.26
Proline(strong)	−0.74	3.00	0.92
Glycine(weak)	−0.34	0.09	0.29
Glycine(strong)	−0.89	3.05	1.28
Glutamine	−0.68	0.09	0.38

1. Proline

The structure of strongly chemisorbed Pro is illustrated in Fig. 4(b), with the circle highlighting the H atom dissociated from Pro. Upon adsorption, the strongly chemisorbed Pro positions itself such that the H atom of its carboxyl group can interact with a –OH group on the $Mg(OH)_2$ layer. The H-atom from the carboxyl on Pro detaches and forms a water-like structure with the –OH group that binds to Mg. The O–Mg separation increases from 2.113 Å for O to the three neighboring Mg atoms in undisturbed $Mg(OH)_2$ to 2.199 Å separation from one Mg atom and no bond (distances exceeding 3.5 Å) to the two other Mg atoms. The dissociation and water formation indicate that the deformation energies in Table II also include the dissociation energy of the H atom from Pro and the change in the –OH group on $Mg(OH)_2$. The more weakly chemisorbed Pro does not deform the surface or itself as strongly. While the deformation energies differ much between the weakly and strongly chemisorbed situation for Pro, the difference in E_{ads} is only ≈300 meV.

Although the zwitterionic form of Pro is unstable when isolated in vacuum (as also verified by us), we test changing the weakly adsorbed Pro found here into zwitterionic Pro by moving the carboxyl H atom to N and changing the starting charges on the left-out O and on N. We then let the system further relax, still with a vacuum above, and find that it ends up in a structure like Fig. 4(a)—the ordinary Pro weakly adsorbed and with the same value of E_{ads}.

2. Glycine

Gly also adsorbs both in a weak chemisorption [Fig. 4(c)], and in a stronger chemisorption with dissociation of a H atom from the

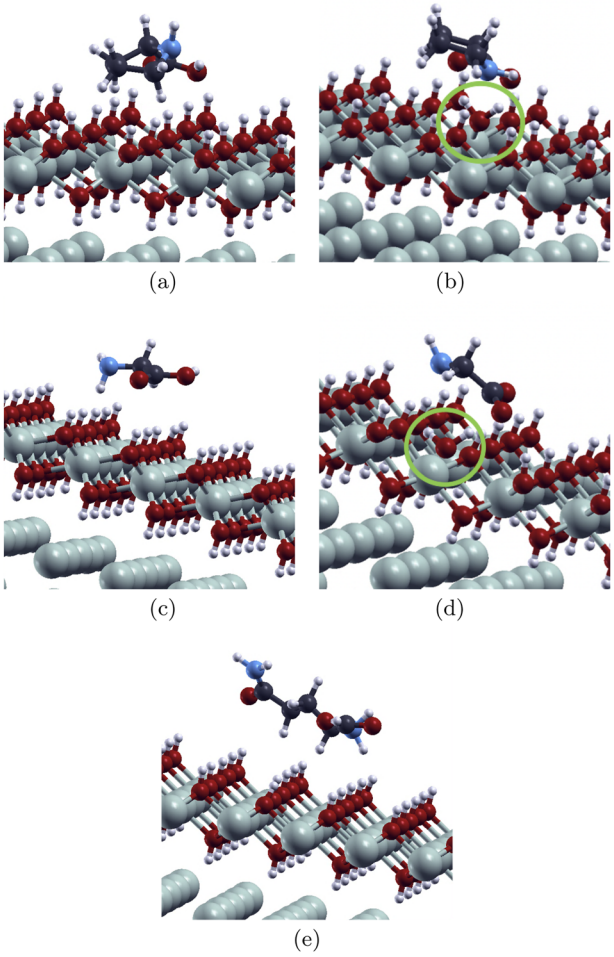

FIG. 4. Amino acids interacting with $Mg(OH)_2$ on Mg(0001). (a) Weakly chemisorbed proline. (b) Strongly chemisorbed proline. (c) Weakly chemisorbed glycine. (d) Strongly chemisorbed glycine. (e) Glutamine. The circles in (b) and (d) indicate the position of the H atom dissociated from the amino acid.

carboxyl group on Gly [Fig. 4(d)]. Both structures are stable, but the deformation energies involved in the dissociation are, as expected, more than an order of magnitude larger, see Table II. Again, a water-like structure forms on $Mg(OH)_2$ by the H from Gly attaching to a –OH group on $Mg(OH)_2$, with O–Mg distance changing to 2.198 Å, similar to the Pro case. Again, we also tested to change the weakly adsorbed Gly molecule to zwitterionic and let the system further relax. For Gly, the system ends up in the same structure as for the strongly adsorbed Gly molecule and with the same value of $E_{ads} = -0.89$ eV/molecule.

In Ref. 40, the adsorption of zwitterionic glycine on $Mg(OH)_2$ in vacuum was also studied. The adsorption energy found there was larger, at ≈ -3 eV/molecule, despite the third H atom on N not dissociating. This is likely due to a combination of differences to our study: The value of E_{cut} used there is low (at 25 Ry), the coverage of Gly is larger (with one Gly in a 3×3 surface unit cell compared to our one molecule per 5×5 surface unit cell), and not least, it seems from the description that the $E_{adsorbant}$ for the isolated Pro is in their case somehow the zwitterionic form of Pro, which (if at all possible to stabilize in isolated form) will have a large energy in vacuum compared to the normal Pro. That would then lead to a large gain in energy at adsorption, even without dissociation of the H atom. We find it difficult to compare our result to that of Ref. 40.

3. Glutamine

For Gln, we find a number of similar adsorption structures, illustrated by one of them in Fig. 4(e). However, despite many different starting positions for the optimization of the adsorption structure, including some with the –OH group of carboxyl placed close to the surface, none of the calculations result in dissociation of the H atom from Gln. Furthermore, Table II shows that there is merely a small change in the deformation energy of both the surface and Gln when they interact. In other words, the adsorption and deformation energies remain the same or similar at the end of each calculation, regardless of how the molecule is initially positioned.

Gly and Pro are smaller molecules than Gln and face less steric hindrance at adsorption, making both weak and strong chemisorption possible. This is also seen when Gly adsorbs directly on the metal surface of Mg(0001),[29] although, in that study, the difference in adsorption energy for the two cases is minute.

The dehydration of $Mg(OH)_2$ that Pro and Gly thus contribute to is interesting because, in itself (no added amino acids), this process has a very slow reaction rate at body temperatures,[41] but Pro and Gly adsorption increases the chances. At the same time, dehydration could result in the formation of a pit in $Mg(OH)_2$, exposing the Mg surface to the environment and the start of a corrosion pit in Mg.

The difference in adsorption for Gly and Pro in either the weakly or strongly chemisorbed structures resembles adsorption of methanol (with –OH group) and methoxy (with lone-pair O) on surfaces of chromia [specifically on the α-Cr_2O_3(0001) surface] and alumina [on the α-Cr_2O_3(0001) surface].[42,43] In those studies, one of us found that the two molecules, differing only by the missing hydroxyl H atom on methoxy, adsorb very differently. Methanol adsorbs "passively" on α-Cr_2O_3(0001), with atomic structure almost unchanged and with adsorption energy −0.8 eV/molecule, whereas methoxy shows a strong surface–adsorbate interaction, with the methoxy O atom strongly bonded to the surface and with an adsorption energy −3.3 eV/molecule. With the cost 2.4 eV of dissociating the H atom from gas phase methanol and leaving it as part of a H_2 molecule,[42] this is energetically just barely possible on α-Cr_2O_3(0001), unless the gain of adsorbing the dissociated H atom onto α-Cr_2O_3(0001) instead outweighs the dissociation cost (this was not studied in Ref. 42).

In this study, the dissociated H atom in Pro and Gly strong binding adsorbs separately on $Mg(OH)_2$, and the system gains energy compared to adsorption without dissociating ("weak"), by 0.3–0.6 eV/molecule [Table II]. The dissociation cost, which is implicitly part of the energy here, is a cause for this relatively small difference in adsorption energy.

C. Effect on the $Mg(OH)_2$/Mg(0001) interaction

With the amino acids adsorbing so differently on $Mg(OH)_2$, one could expect the effect to progress further into the surface to

TABLE III. Adsorption energy of a 5 × 5 layer of $Mg(OH)_2$ adsorbed on Mg(0001), with one molecule of the indicated amino acid or a second layer of $Mg(OH)_2$ adsorbed on top of $Mg(OH)_2$. Values in eV per adsorbed amino acid (and 5 × 5 surface unit cell).

Amino acid on $Mg(OH)_2$/Mg(0001)	E_{ads}
None	−3.95
Proline(weak)	−3.87
Proline(strong)	−3.86
Glycine(weak)	−3.86
Glycine(strong)	−3.83
Glutamine	−3.87
Second layer $Mg(OH)_2$	−4.45

affect how the $Mg(OH)_2$ layer binds to Mg(0001). One could also expect that the effect would depend on which amino acid, if any, is adsorbed on top, as well as the strength of the adsorption.

Table III reports the difference in adsorption energies of $Mg(OH)_2$ on Mg(0001). The results show that (i) adsorbing an amino acid on $Mg(OH)_2$ weakens the $Mg(OH)_2$–Mg(0001) binding energy by less than 120 meV per 5 × 5 unit cell (3%) and, thus, per molecule, and (ii) the type of amino acid and strength of adsorption on the $Mg(OH)_2$ layer hardly matters for the adsorption energy between $Mg(OH)_2$ and Mg(0001), with difference less than 40 meV/molecule, or 1%. Thus, despite the change in atomic and electron structure on the top of $Mg(OH)_2$ when Gly or Pro provides a H atom in strong chemisorption, it does not affect the binding of $Mg(OH)_2$ to Mg(0001), compared to the weakly adsorbed molecules.

A second layer of $Mg(OH)_2$ on top of the initial layer has the effect that $Mg(OH)_2$ binds stronger to Mg(0001), but only by about 500 meV per 5 × 5 surface unit cell (13%) compared to a single layer on Mg(0001), while the $Mg(OH)_2$–$Mg(OH)_2$ binding is much stronger, at 12 eV, for the same area (480 meV per 1 × 1 surface cell). These results also show that it only requires a few layers of $Mg(OH)_2$ before it is energetically much better for $Mg(OH)_2$ in bulk rather than adsorbed to Mg. While the $Mg(OH)_2$ layer on Mg(0001) may have an entirely different origin than being cut out from bulk $Mg(OH)_2$ (e.g., created on top of the Mg surface by corrosion of Mg), once more $Mg(OH)_2$ layers are formed one can envision a reverse process: multiple layers of $Mg(OH)_2$ lifting off the Mg(0001) surface. We speculate that, as more layers adsorb on top (at a gain of ~12 eV per layer), the bulk-like structure thus formed will eventually be ripped off or slide off, leaving the Mg surface again unprotected. Thus, the $Mg(OH)_2$ layers act as temporary protection, but one must look into further protection to keep the corrosion speed reasonably slow for implant purposes.

D. Effects of possible alloying of Mg(0001)

In this study, we have focused on the pristine Mg(0001) surface. It is well known that alloying Mg with small amounts of zinc (Zn) and calcium (Ca) improves the corrosion resistance,[44] while still keeping the surface biocompatible.[9,44] In a previous study, we examined amino acids on pristine and alloyed Mg(0001)[29] and found that the adsorption energy increases with sparse alloying of the surface and the molecules move such that an O atom is positioned above the Ca atom, or above a Mg atom, that is nearest neighbor to the Zn atom. In other words, the precise positioning of the molecule on the surface becomes important with alloys.

We see a similar effect in Ref. 45, where a layer of hydroxyapatite (HAp) is adsorbed on top of pristine or alloyed Mg(0001). There, the adsorption energy of the HAp layer generally increases with alloying, except for specific relative positions of the HAp layer relative to the Mg surface, e.g., when a Ca (phosphorus) atom of HAp is put directly above a Ca (Zn) alloying atom. Further studies on the effect of alloying on the adsorption have been carried out in Refs. 46 and 47. From the set of these studies, we find that one can expect the adsorption energies presented here to improve with alloying of the Mg(0001) surface, especially the Mg(0001)-to-$Mg(OH)_2$ interaction, although by less than 50% (and likely rather in the 5%–20% range), as judged from the adsorption energy changes reported in Refs. 29 and 45. Explicit calculations of this are left for a future study.

IV. SUMMARY

This study provides a detailed analysis of the interface of a layer of $Mg(OH)_2$ with Mg(0001) and the changes at adsorption of amino acids that are relevant in the environment of Mg-based implants. Using a potential energy surface plot, we find the optimal adsorption position of $Mg(OH)_2$ on Mg(0001). The associated adsorption energy is −17.9 meV/Å, and the corrugation, estimated from the difference between the largest and smallest adsorption energies of any position, is small with a value of 5.7 meV/Å. Thus, we conclude that $Mg(OH)_2$ is both relatively easy to peel off (at a lower adsorption energy than graphene on graphite) and can easily slide on top of Mg(0001).

Our study further shows that glycine, proline, and glutamine interact with the $Mg(OH)_2$ layer to varying extents, with glycine and proline adsorbing in both weak and strong chemisorption. For glycine and proline, the strong chemisorption increases the deformation energies of $Mg(OH)_2$ and the molecule itself significantly, while the adsorption energies are less affected. This increase is attributed to the dissociation of a H atom from the amino acid carboxyl group, moving to a –OH group on $Mg(OH)_2$ to form a water-like structure, although still attached to one Mg atom in $Mg(OH)_2$. In contrast, glutamine does not show dissociation of its carboxyl group.

The presence of amino acids on $Mg(OH)_2$ is found to have little impact on the adsorption energy of $Mg(OH)_2$ on Mg(0001). Adding another layer of $Mg(OH)_2$ affects the $Mg(OH)_2$–Mg(0001) binding more, but the strength of $Mg(OH)_2$–Mg(0001) stays at orders of magnitude smaller than the binding energy of layers within the bulk of $Mg(OH)_2$.

Our work shows that, while $Mg(OH)_2$ may form due to corrosion of the Mg surface, it is relatively easy to remove, and this does not change significantly with interaction of amino acids or formation of further $Mg(OH)_2$ layers. Our study shows that $Mg(OH)_2$ does not protect the Mg surface sufficiently for an efficient coating by itself.

SUPPLEMENTARY MATERIAL

The final coordinates for the structures presented here are available as supplementary material.

ACKNOWLEDGMENTS

The authors would like to thank D. Orlov (Lund) and P. Maier (Stralsund) for discussions. This work was supported by the Swedish Research Council (VR) through Grant No. 2020-04997 and by Chalmers Area of Advance (AoA) Nano and AoA Materials. The computations were performed using computational and storage resources at Chalmers Center for Computational Science and Engineering (C3SE), and with computer and storage allocations from the National Academic Infrastructure for Supercomputing in Sweden (NAISS), under Contract Nos. NAISS2024/3-16, NAISS2024/6-432, NAISS2025/3-25, and NAISS2025/5-484.

AUTHOR DECLARATIONS

Conflict of Interest

The authors have no conflicts to disclose.

Author Contributions

S.A., M.E., L.H., and D.N. contributed equally to this work.

Miranda Naurin: Conceptualization (equal); Formal analysis (supporting); Investigation (lead); Visualization (equal); Writing – original draft (equal). **Sally Aldhaim**: Conceptualization (equal); Investigation (supporting); Writing – review & editing (equal). **Moltas Elliver**: Conceptualization (equal); Investigation (supporting); Writing – review & editing (equal). **Ludwig Hagby**: Conceptualization (equal); Investigation (supporting); Writing – review & editing (equal). **J. Didrik Nilsson**: Conceptualization (equal); Investigation (supporting); Writing – review & editing (equal). **Elsebeth Schröder**: Conceptualization (equal); Data curation (equal); Formal analysis (lead); Funding acquisition (equal); Investigation (supporting); Resources (equal); Supervision (equal); Validation (equal); Writing – original draft (equal).

DATA AVAILABILITY

The atomic positions used in our calculations are available as supplementary material.

APPENDIX: CONVERGENCE OF k-POINTS AND ENERGY CUTOFFS

To estimate the k-point sampling needed for a 1 × 1 surface unit cell, we calculated the total energy of $Mg(OH)_2$ on top of Mg(0001), with all atomic positions locally optimized, and studied the energy cost ΔE of lifting the $Mg(OH)_2$ layer 0.1 Å from Mg(0001), with all atoms in fixed positions. For the convergence study of the k-point sampling, we use 50/400 Ry energy cutoff values for plane-wave density and electron density E_{cut} and E^{ρ}_{cut}. The results for the k-point samplings $k \times k \times 1$ with k = 10, 18, 20, 24, and 30 are shown in Fig. 5 (top). We find that, with 18 × 18 × 1, the calculations are sufficiently converged, with 0.03 meV/Å^2 deviation from the asymptote, while the 10 × 10 × 1 sampling converges the results to 0.3 meV/Å^2 away from the asymptote. As discussed in the main text, we use the more dense sampling for $Mg(OH)_2$ on Mg(0001) calculations, while for amino acid adsorption, the more sparse choice is sufficient.

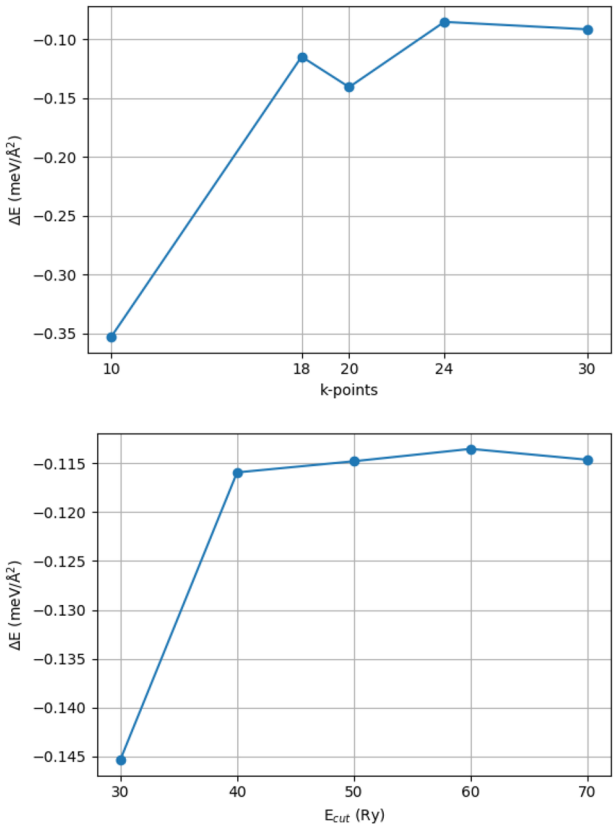

FIG. 5. Convergence study of k-point sampling (top) and energy cutoff values E_{cut} with E^{ρ}_{cut} = 8 E_{cut} (bottom). Calculated energy differences ΔE between $Mg(OH)_2$ adsorbed on Mg(0001) and the layer translated to 0.1 Å above Mg(0001), without further relaxing the atomic positions.

With a similar procedure, we determined the energy cutoff values E_{cut} and E^{ρ}_{cut} for the plane-wave densities and the charge density, at 18 × 18 × 1 k-point sampling, as shown in Fig. 5 (bottom). We concluded that 50/400 Ry is sufficient for the project with the present choice of pseudopotentials and exchange-correlation approximation.

REFERENCES

[1] C. H. Hung, Y. C. Kwok, J. Yip, H. H. Wong, and Y. Y. Leung, "Bioabsorbable magnesium-based materials potential and safety in bone surgery: A systematic review," Craniomaxillofacial Trauma Reconstr. **18**, 24 (2025).
[2] V. Tsakiris, C. Tardei, and F. M. Clicinschi, "Biodegradable Mg alloys for orthopedic implants—A review," J. Magnesium Alloys **9**, 1884–1905 (2021).
[3] T. Kim, C. W. See, X. Li, and D. Zhu, "Orthopedic implants and devices for bone fractures and defects: Past, present and perspective," Eng. Regener. **1**, 6–18 (2020).
[4] T. Kraus, S. F. Fischerauer, A. C. Hänzi, P. J. Uggowitzer, J. F. Löffler, and A. M. Weinberg, "Magnesium alloys for temporary implants in osteosynthesis: In vivo studies of their degradation and interaction with bone," Acta Biomater. **8**(3), 1230–1238 (2012).
[5] F. Witte, V. Kaese, H. Haferkamp, E. Switzer, A. Meyer-Lindenberg, C. J. Wirth, and H. Windhagen, "In vivo corrosion of four magnesium alloys and the associated bone response," Biomaterials **26**, 3557–3563 (2005).

[6]B. J. Luthringer, F. Feyerabend, and R. Willumeit-Römer, "Magnesium-based implants: A mini-review," Magnesium Res. **27**, 142–154 (2014).
[7]S. Agarwal, J. Curtin, B. Duffy, and S. Jaiswal, "Biodegradable magnesium alloys for orthopaedic applications: A review on corrosion, biocompatibility and surface modifications," Mater. Sci. Eng.: C **68**, 948–963 (2016).
[8]H. Ben Amara, J. Philip, O. Omar, and P. Thomsen, "Gas bubbles from biodegradable magnesium implants convey mechanical cues and promote immune cell stimulation," Adv. Sci. **12**, 2503123 (2025).
[9]A. Mohamed, A. M. El-Aziz, and H.-G. Breitinger, "Study of the degradation behavior and the biocompatibility of Mg–0.8Ca alloy for orthopedic implant applications," J. Magnesium Alloys **7**, 249–257 (2019).
[10]Quantum ESPRESSO Manifesto, 2021, URL https://www.quantum-espresso.org/manifesto/.
[11]P. Giannozzi, S. Baroni, N. Bonini, M. Calandra, R. Car, C. Cavazzoni, D. Ceresoli, G. L. Chiarotti, M. Cococcioni, I. Dabo, A. Dal Corso, S. de Gironcoli, S. Fabris, G. Fratesi, R. Gebauer, U. Gerstmann, C. Gougoussis, A. Kokalj, M. Lazzeri, L. Martin-Samos, N. Marzari, F. Mauri, R. Mazzarello, S. Paolini, A. Pasquarello, L. Paulatto, C. Sbraccia, S. Scandolo, G. Sclauzero, A. P. Seitsonen, A. Smogunov, P. Umari, and R. M. Wentzcovitch, "QUANTUM ESPRESSO: A modular and open-source software project for quantum simulation of materials," J. Phys.: Condens. Matter **21**, 395502 (2009).
[12]P. Giannozzi, O. Andreussi, T. Brumme, O. Bunau, M. Buongiorno Nardelli, M. Calandra, R. Car, C. Cavazzoni, D. Ceresoli, M. Cococcioni, N. Colonna, I. Carnimeo, A. Dal Corso, S. de Gironcoli, P. Delugas, R. A. DiStasio, A. Ferretti, A. Floris, G. Fratesi, G. Fugallo, R. Gebauer, U. Gerstmann, F. Giustino, T. Gorni, J. Jia, M. Kawamura, H.-Y. Ko, A. Kokalj, E. Küçükbenli, M. Lazzeri, M. Marsili, N. Marzari, F. Mauri, N. L. Nguyen, H.-V. Nguyen, A. Otero-de-la-Roza, L. Paulatto, S. Poncé, D. Rocca, R. Sabatini, B. Santra, M. Schlipf, A. P. Seitsonen, A. Smogunov, I. Timrov, T. Thonhauser, P. Umari, N. Vast, X. Wu, and S. Baroni, "Advanced capabilities for materials modelling with quantum ESPRESSO," J. Phys.: Condens. Matter **29**(46), 465901 (2017).
[13]M. Dion, H. Rydberg, E. Schröder, D. C. Langreth, and B. I. Lundqvist, "van der Waals density functional for general geometries," Phys. Rev. Lett. **92**(24), 246401 (2004).
[14]E. Schröder, V. R. Cooper, K. Berland, B. I. Lundqvist, P. Hyldgaard, and T. Thonhauser, "Chapter 8—The vdW-DF family of nonlocal exchange-correlation functionals," in *Non-Covalent Interactions in Quantum Chemistry and Physics*, edited by A. Otero de la Roza and G. A. DiLabio (Elsevier, 2017), pp. 241–274.
[15]K. Berland and P. Hyldgaard, "Exchange functional that tests the robustness of the plasmon description of the van der Waals density functional," Phys. Rev. B **89**, 035412 (2014).
[16]K. Berland, C. A. Arter, V. R. Cooper, K. Lee, B. I. Lundqvist, E. Schröder, T. Thonhauser, and P. Hyldgaard, "van der Waals density functionals built upon the electron-gas tradition: Facing the challenge of competing interactions," J. Chem. Phys. **140**(18), 18A539 (2014).
[17]K. Berland, V. R. Cooper, K. Lee, E. Schröder, T. Thonhauser, P. Hyldgaard, and B. I. Lundqvist, "van der Waals forces in density functional theory: a review of the vdW-DF method," Rep. Prog. Phys. **78**, 066501 (2015).
[18]P. E. Blöchl, "Projector augmented-wave method," Phys. Rev. B **50**, 17953 (1994).
[19]A. Dal Corso, "Pseudopotentials periodic table: From H to Pu," Comput. Mater. Sci. **95**, 337 (2014).
[20]Z. Xing, D. Orlov, and E. Schröder, "Tailored pseudopotentials for magnesium surface core level shift calculations," Phys. Rev. Mater. **8**, 123801 (2024).
[21]A. Dal Corso, "PSLibrary: A library of ultrasoft and PAW pseudopotentials," available at: https://dalcorso.github.io/pslibrary/ (January 2026).
[22]H. J. Monkhorst and J. D. Pack, "Special points for Brillouin-zone integrations," Phys. Rev. B **13**, 5188 (1976).
[23]M. D. Hanwell, D. E. Curtis, D. C. Lonie, T. Vandermeersch, E. Zurek, and G. R. Hutchison, "Avogadro: An advanced semantic chemical editor, visualization, and analysis platform," J. Cheminf. **4**, 17 (2012).
[24]D. Steiner Petrovič, D. Mandrino, B. Šarler, J. Horky, A. Ojdanic, M. J Zehetbauer, and D. Orlov, "Surface analysis of biodegradable Mg-alloys after immersion in simulated body fluid," Materials **13**, 1740 (2020).
[25]R. Willumeit, J. Fischer, F. Feyerabend, N. Hort, U. Bismayer, S. Heidrich, and B. Mihailova, "Chemical surface alteration of biodegradable magnesium exposed to corrosion media," Acta Biomater. **7**, 2704–2715 (2011).
[26]M. Tomozawa and S. Hiromoto, "Growth mechanism of hydroxyapatite-coatings formed on pure magnesium and corrosion behavior of the coated magnesium," Appl. Surf. Sci. **257**, 8253–8257 (2011).
[27]T. Ishizaki, S. Chiba, K. Watanabe, and H. Suzuki, "Corrosion resistance of Mg–Al layered double hydroxide container-containing magnesium hydroxide films formed directly on magnesium alloy by chemical-free steam coating," J. Mater. Chem. A **1**, 8968–8977 (2013).
[28]D. Zhang, P. Zhang, S. Song, Q. Yuan, P. Yang, and X. Ren, "Simulation of magnesium hydroxide surface and interface," J. Alloys Compd. **612**, 315–322 (2014).
[29]J. Bolin, A. Goold, O. Hildeberg, A. Limbäck, and E. Schröder, "A DFT study of amino acids on Mg and Mg-based alloys," arXiv:2601.07680 (2026).
[30]L. Bengtsson, "Dipole correction for surface supercell calculations," Phys. Rev. B **59**(19), 12301–12304 (1999).
[31]M. Catti, G. Ferraris, S. Hull, and A. Pavese, "Static compression and H disorder in brucite, $Mg(OH)_2$, to 11 GPa: A powder neutron diffraction study," Phys. Chem. Miner. **22**, 200–206 (1995).
[32]J. Åkesson, O. Sundborg, O. Wahlström, and E. Schröder, "A van der Waals density functional study of chloroform and other trihalomethanes on graphene," J. Chem. Phys. **137**(17), 174702 (2012).
[33]R. Naomi, P. M. Ridzuan, and H. Bahari, "Current insights into collagen type I," Polymers **13**(16), 2642 (2021).
[34]X. Nie, X. Sun, C. Wang, and J. Yang, "Effect of magnesium ions/type I collagen promote the biological behavior of osteoblasts and its mechanism," Regener. Biomater. **7**, 53–61 (2019).
[35]A. D. Theocharis, S. S. Skandalis, C. Gialeli, and N. K. Karamanos, "Extracellular matrix structure," Adv. Drug Delivery Rev. **97**, 4–27 (2016).
[36]J. C. Hall, K. Heel, and R. McCauley, "Glutamine," Br. J. Surg. **83**, 305–312 (1996).
[37]V. F. Cruzat, "Chapter 18—Glutamine and skeletal muscle," in *Nutrition and Skeletal Muscle*, edited by S. Walrand (Academic Press, 2019), pp. 299–313.
[38]N. Jacobson, B. Tegner, E. Schröder, P. Hyldgaard, and B. Lundqvist, "Hydrogen dynamics in magnesium and graphite," Comput. Mater. Sci. **24**, 273–277 (2002).
[39]T. Jiang, L.-X. Sun, and W.-X. Li, "First-principles study of hydrogen absorption on Mg(0001) and formation of magnesium hydride," Phys. Rev. B **81**, 035416 (2010).
[40]X. Tang, Z. Du, Y. Wang, Y. Zhu, C. Unluer, and P. Liu, "Structure-induced enhanced dissolving properties of $Mg(OH)_2$ prepared by glycine-assisted MgO hydration," Cryst. Res. Technol. **58**, 2300074 (2023).
[41]Y. Youn, T. W. Kim, K. Cho, and S. K. Hong, "Investigation on the initial stage of the dehydration process in $Mg(OH)_2$ by density functional theory calculations," ACS Appl. Mater. Interfaces **16**(18), 23122–23129 (2024).
[42]Ø. Borck and E. Schröder, "Adsorption of methanol and methoxy on the α-Cr_2O_3(0001) surface," J. Phys.: Condens. Matter **18**, 10751 (2006).
[43]Ø. Borck and E. Schröder, "First-principles study of the adsorption of methanol at the α-Al_2O_3(0001) surface," J. Phys.: Condens. Matter **18**, 1 (2006).
[44]M. Behera, A. Denys, R. Shabadi, F. Allain, and C. Gruescu, "Micro-alloying of Zn and Ca in vacuum induction casted bioresorbable Mg system: Perspectives on corrosion resistance, cytocompatibility, and inflammatory response," J. Magnesium Alloys **12**, 2812 (2024).
[45]A. Veit Berg, A. Forster, T. Hansson, A. J. Jernstedt, E. Salminen, and E. Schröder, "First-principle study of the influence of hydroxyapatite on magnesium surfaces," arXiv:2603.19823 (2026).
[46]M. Esmaily, J. E. Svensson, S. Fajardo, N. Birbilis, G. S. Frankel, S. Virtanen, R. Arrabal, S. Thomas, and L. G. Johansson, "Fundamentals and advances in magnesium alloy corrosion," Prog. Mater. Sci. **89**, 92–193 (2017).
[47]Z. Fang, J. Wang, S. Zhu, X. Yang, Y. Jia, Q. Sun, and S. Guan, "A DFT study of the adsorption of short peptides on Mg and Mg-based alloy surfaces," Phys. Chem. Chem. Phys. **20**, 3602–3607 (2018).